Received: 12 November 2019 | Revised: 3 January 2020 | Accepted: 13 January 2020

DOI: 10.1002/aoc.5566

FULL PAPER

Applied Organometallic Chemistry WILEY

Transition Metal–organic Coordination Polymers Containing 6-(1H-imidazol-1-yl)-2(1H)-Pyridinone: Synthesis, Structure and Fluorescent Sensing for Enoxacin

Shanshan Li | **Xin Zhou** | **Qiwei Xu** | **Dongmei Liu** | **Ruifang Cui** | **Xia Li**

Department of Chemistry, Capital Normal University, Beijing, 100048, China

Correspondence
Xia Li, Department of Chemistry, Capital Normal University, Beijing, 100048, China.
Email: xiali@cnu.edu.cn

Funding information
Laboratory Open Project Fund of Capital Normal University, Grant/Award Number: LIP18009S047; National Natural Science Foundation of China, Grant/Award Number: 21471104; Beijing Education Commission, Grant/Award Number: KZ201910028038

Three metal–organic coordination polymers, [M(2,6-bip)$_2$] (M = Zn (**1**), Ni (**2**)) and [Cu (tfbdc)(2,6-bipH)$_2$]•2H$_2$O (**3**), were obtained with the similar solvothermal reaction systems of bivalent transition metal salt, 6-(1H-imidazol-1-yl)-2(1H)-pyridinone (2,6-bipH) and 2,3,5,6-tetrafluoroterephthalic acid (H$_2$tfbdc). The three coordination polymers show different framework features, namely 3D (**1**), 2D (**2**) and 1D (**3**) structures, which are resulted from different single-metal ion “node” and “linker” coordination modes. The [ZnO$_2$N$_2$] tetrahedron in **1** and [NiO$_2$N$_4$] octahedron in **2** as a node, is formed from Zn sp^3 and Ni d^{2}sp^3 hybrid orbits, respectively, while the linker, 2,6-bip, adopts the μ_2:$\eta^1\eta^1\eta^0$ in **1** and μ_2:$\eta^1\eta^1\eta^1$ in **2** coordination modes. PLATON calculation suggests that **1** possesses the micropore structure with a pore volume of 14.2%. In **3**, the [CuO$_2$N$_2$] parallelogram as a node is derived from Cu dsp^3 hybrid orbital, while the linkers of 2,6-bipH and tfbdc adopt the μ_1:$\eta^1\eta^0\eta^0$ and μ_1:$\eta^1\eta^0$/μ_1:$\eta^1\eta^0$ coordination modes, respectively. Intriguingly, Zn(d^{10})-centre coordination polymer **1** shows strong blue emission, which are derived from the $\pi^* \rightarrow \pi$ transition of the 2,6-bipH ligand. Moreover, **1** exhibits high stability and strong luminescence in both water and ethanol. At this point, the performance of **1** is studied as a chemical sensor for detecting fluoroquinolones drug. The results show that **1** can detect enoxacin in ethanol solution with a low detection limit of 3.61×10^{-5} M. The luminescent sensing mechanisms were investigated from experimental methods and theoretical calculation in detail as well.

KEYWORDS

Enoxacin, luminescent sensing, metal–organic coordination polymers, structure

1 | INTRODUCTION

Metal–organic coordination polymers (CPs) are prepared by inorganic building units and linkers through coordination bonds, which show a variety of structures and unique physical/chemical properties. These materials have already shown potential applications in adsorption, separation, catalysis, luminescence and chemical sensing, etc.[1–7] The structures of CPs vary from 1D to 3D extended frameworks, including open or porous structures.[8,9] The CPs are often obtained by means of secondary building units (SBUs) and multitopic ligands, the connections between linkers and metal ions could extend in space and form the coordination frameworks.[10,11]

The basic SBUs are composed of metal ions or clusters, such as the single-metal ion "node", binuclear clusters, trinuclear metal clusters, or polynuclear clusters.[12,13] The strong coordination bond between SBUs and linkers can make the frameworks rigid, stable and amenable to further development for industrial applications.[14] Various design and synthesis approaches were developed to construct CPs, and the variability of lanthanide or transition metal–ligand combinations led to numerous CPs materials.[15,16] CPs have a diversity of structures since multiple coordination environments of transition metal ions. For example, Zn, Cu, Cd, Ni, and Co can adopt four-, five-, or six-coordinate geometries, leading to the extended CPs from 1D to 3D dimensionality[8–12,14,17–20] However, CPs based on the transition metal ions without unpaired electrons, especially those with d^{10} configurations of Zn/Cd, can yield linker-based high emission.[11,21] So, the Zn/Cd-luminescence coordination polymers were studied for luminescence sensing of the analytes.[11,22–24] In recent years, the luminescence has been widely employed in analytical, environment, and biomedical applications.[1,4,13,25–27] Luminescent CPs have been reported as fluorescent sensors for the detection of anions, cations, organic small molecules and gas molecules.[11,22–25,28,29]

Enoxacin (EX) is an important synthetic antibiotic, which belongs to fluoroquinolones (FQs). FQs are mainly used for the treatment of respiratory tract infections and special infections caused by gram-negative and gram-positive bacteria.[30] However, their abused usage can lead to potential residual in animal-derived food matrices, causing adverse reactions and reducing the efficiency of human infection treatment. Therefore, the development of effective FQs detecting method is urgent. Compared with instrumental analysis method,[31–34] fluorescence FQ detection may be a promising method due to its high sensitivity and simple sample preparation procedures. Therefore, it is important to develop luminescent CPs as the sensor for EX detection.

Multi-functional organic ligands play an important role in the luminescence of CPs. To the best of our knowledge, organic ligands with a π-conjugated system can enhance the stability of CPs, and improve the luminescence properties due to their conjugation effects and π-π* transitions.[13,35,36] Aromatic compounds, such as aromatic polycarboxylic acid and/or N-donor auxiliary ligands are used in synthesis of the coordination polymers with good luminescence properties.[2,12,37–44] 1,4-benzenedicarboxylic acid (1,4-BDC) is widely used in CPs,[39,42,44] and its derivative ligand 2,3,5,6-tetrafluoroterephthalic acid (H_2tfbdc) is seldom investigated.[42–44] H_2tfbdc, like 1,4-BDC, is also utilized as the linker to form open frameworks. Furthermore, H_2tfbdc is a fluorinated aromatic dicarboxylic acid. Fluorinated organic ligands can improve the luminescence of the coordination polymers by reducing the fluorescence quenching effect due to the vibrational C-H bonds.[44] The hydroxylation of N-heterocyclic ligand, 6-(1H-imidazol-1-yl)-2(1H)-Pyridinone (2,6-bipH) contains N/O-donor atoms with a π-conjugated system, which can act as a linker and bridge metal atoms in the construction of coordination frameworks.

Considering these points, H_2tfbdc/2,6-bipH as ligands and transition metal Zn/Ni/Cu with different constructions to synthesize coordination polymers. So, three new coordination frameworks, $[M(2,6\text{-bip})_2]$ (M = Zn(**1**), Ni(**2**)) and $[Cu\ (tfbdc)(2,6\text{-bipH})_2]\bullet 2H_2O$(**3**) were obtained under hydrothermal reaction conditions. Zn, Ni, and Cu adopt different constructions, Zn sp^3, Ni d^2sp^3, and Cu dsp^2 hybrid orbitals, the $[ZnO_2N_2]$ tetrahedron, $[NiO_2N_4]$ octahedron, and $[CuO_2N_2]$ parallelogram are formed, which can be incorporated into the single-metal ion node as building unit. Linker 2,6-bipH adopt different coordination modes in **1–3**. The combinations of single-metal ion node and the linkers create the coordination polymer formation of the 3D (**1**), 2D (**2**), and 1D (**3**). Intriguingly, Zn(d^{10})-centre coordination polymer **1** exhibits strong linker-based luminescence. Thus, coordination polymer **1** as a luminescence sensor for detecting antibiotics was studied. Luminescence sensing for EX was realized by luminescence quenching effect and the sensing mechanism was investigated in detail as well, which indicates a potential application in chemical sensing.

2 | EXPERIMENTAL

2.1 | Materials and physical measurements

Zn $(CH_3COO)_2$, $NiSO_4\bullet 6H_2O$, $CuCl_2$, 2,6-bipH and H_2tfbdc were commercially available. The C, H, N elemental analysis data of **1–3** were determined by the Vario EL III elemental analyzer of Elementar Company of Germany. Infrared (IR) spectra were obtained on a Bruker Tensor 37 spectrophotometer (KBr pellet). Experimental powder X-ray diffraction was measured on a PANalytical X'Pert PRO MPD diffractometer with CuKα radiation. Fluorescence spectra of **1** in solid/liquid state were determined by Hitachi F-7000 fluorescence spectrophotometer. The thermal stability of coordination polymers **1–3** by thermogravimetric analyses (TGA) were measured on a HCT-2 differential thermal analyzer (air atmosphere, a heating rate of 10 $°C\bullet min^{-1}$). UV–vis spectra were obtained on a 2550 UV–visible spectrophotometer (Shimadzu, Kyoto, Japan).

2.2 | Synthesis of coordination polymers 1–3

Coordination polymer **1**: The materials, 2,6-bipH (0.2 mmol), H_2tfbdc (0.2 mmol), Zn $(CH_3COO)_2$ (0.1 mmol), NaOH (0.1 ml, 2 mol•L^{-1}), water (10 ml) and ethanol (2 ml) were placed in a 25 ml Teflon Lined Parr autoclave and heated to 140 °C for 72 hr, then it was cooled to room temperature. Colourless acicular crystals were obtained. Elemental analysis (%) Calcd for $C_{16}H_{12}N_6O_2Zn$: C, 49.81; H, 3.11; N, 21.79. Found: C, 49.87; H, 3.05; N, 21.82. Selected IR (KBr pellet, cm^{-1}): 3420 (w), 3113 (w), 1612 (s), 1548 (m), 1505 (m), 1471 (s), 1387 (w), 1286 (m), 891 (w), 786 (w), 734 (w), 686 (w), 654 (w), 560 (w), 442 (w).

Coordination polymer **2**: The 2,6-bipH (0.2 mmol), H_2tfbdc (0.2 mmol), $NiSO_4$•$6H_2O$ (0.3 mmol), NaOH (0.2 ml, 2 mol•L^{-1}), water (8 ml) and ethanol (2 ml) were placed in a 25 ml Teflon Lined Parr autoclave and heated to 120 °C for 72 hr. After that the reaction mixture was cooled to room temperature. Pale-green block crystals were obtained. Elemental analysis (%) Calcd for $C_{16}H_{12}N_6NiO_2$: C, 50.69; H, 3.17; N, 22.18. Found: C, 50.48; H, 3.13; N, 22.11. IR (KBr pellet, cm^{-1}): 3606 (w), 3436 (w), 2923 (s), 2376 (m), 1612 (m), 1461 (s), 1109 (w), 721 (w), 420 (w).

Cooedination polymer **3**: A mixture of 2,6-bipH (0.2 mmol), H_2tfbdc (0.2 mmol), $CuCl_2$ (0.1 mmol), NaOH (0.2 ml, 1 mol•L^{-1}), water (8 ml) and ethanol (2 ml) were placed in a 25 ml Teflon Lined Parr autoclave and heated to 100 °C for 72 hr. It was cooled to room temperature. Pale-green block crystals were obtained. Elemental analysis (%) Calcd for $C_{24}H_{18}CuF_4N_6O_8$: C, 43.80; H, 2.74; N, 12.77. Found: C, 43.40; H, 2.75; N, 12.79. IR (KBr pellet, cm^{-1}): 3551(w), 3396(w), 3142(w), 1616(s), 1548(m), 1503(m), 1469(s), 1377(w), 1278 (m), 989(w), 876(w), 799(w), 745(w), 648(w), 613(w), 515(w).

2.3 | X-ray crystallographic study

Crystals of suitably sized and transparent coordination polymers **1–3** were picked up and diffracted using an X-ray diffractometer with Mo Kα (λ = 0.071073 nm) (**1**, **3**) or Cu Kα (λ = 0.154184 nm) (**2**) monochromatized by a graphite monochromator as a diffracted light source at room temperature. The crystal structure is solved by the SHELXS 97 and SHELXL 97 programs.[45,46] The coordinates of the hydrogen atoms are determined by the theoretical hydrogenation method, and the full-matrix least-squares method is used to correct the hydrogen atoms and the non-hydrogen atoms by the isotropic and anisotropic temperature factors respectively. The crystallographic data and selected bond lengths and angles of the coordination polymers **1–3** are listed in Tables 1 and 2, respectively.

3 | RESULTS AND DISCUSSIONS

3.1 | Crystal structure

Structure of 1. The single crystal X-ray diffraction study reveals that **1** possesses a 3D structure responding to trigonal system and the space group $R\bar{3}$. As depicted in Figure 1a, the asymmetric unit consists of one Zn (II) ion and two 2,6-bip ligands. The coordination environment of Zn (II) ion is a $[ZnO_2N_2]$ tetrahedron using the Zn sp^3 hybrid orbitals. The Zn (II) center is coordinated by two O atoms (O1 and O2) from two different 2,6-bip ligands with bond distances of 1.957 (4) Å and 1.981(4) Å, respectively, while two N atoms (N3A and N6B) from two different 2,6-bip ligands with bond distances of 2.029(5) Å and 2.035(5) Å. The bond angles at the Zn (II) center (O-Zn-O, O-Zn-N, N-Zn-N) are in the range of 95.42(18) °-133.39(17) °. The H_2tfbdc ligand is not coordinated to Zn (II) ion. The 2,6-bip ligand as a linker adopts the μ_2:$\eta^1\eta^1\eta^0$ coordination mode in which the N atom (on the imidazole ring) and the O atom on the 2,6-bip ligand act as coordinating atoms. The dihedral angle between the imidazole ring and the pyridone ring is 10.049(495) ° . The $[ZnO_2N_2]$ units as nodes are bridged by 2,6-bip linkers with a Zn ... Zn distance of 6.276 (13) Å to from the 3D structure. The Right/Left-Zn-(2,6-bip) helical chains exist in the structure due to the deformation of the ligand (Figure 1b). In the helical chain, a repeated unit consist of three Zn (II) centers and three 2,6-bip ligands with the pitch of 14.5084(19) Å and 16.5660 (51) Å. The helical chains are bridged by 2,6-bip ligands resulting in the 3D framework of **1** (Figure 1c). PLATON[47] calculation suggests that the coordination polymer has micropore with the pore volume of 14.2%.

Structure of 2. Coordination polymer **2** is a 2D network structure and crystallizes in monoclinic system and space group $P2_1/c$ with one Ni (II) and two 2,6-bip ligands in the asymmetric unit (Figure 2a). The H_2tfbdc molecule does not participate in the coordination with Ni (II). The arrangement of coordination atoms around the Ni (II) ion displays a $[NiO_2N_4]$ distorted octahedron, which is formed from Ni d^{2}sp^3

TABLE 1 Crystal data and structural refinement for coordination polymers **1–3**

Coordination polymers	1	2	3
Empirical formula	$C_{16}H_{12}N_6O_2Zn$	$C_{16}H_{12}N_6NiO_2$	$C_{24}H_{18}CuF_4N_6O_8$
Formula weight	385.69	379.03	657.98
Temperature/K	296.15	173.00(10)	293(2)
Wavelength/Å	0.71073	1.54184	0.71073
Crystal system	Trigonal	Monoclinic	Triclinic
space group	$R\bar{3}$	$P2_1/c$	$P\bar{1}$
a/Å	23.238(3)	7.38530(10)	7.449(12)
b/Å	23.238(3)	10.5505(2)	7.998(12)
c/Å	16.566(5)	9.34560(10)	11.002(17)
α/°	90	90	103.26(5)
β/°	90	96.7670(10)	95.70(4)
γ/°	120	90	90.58(5)
V/Å^3	7747(3)	723.123(19)	634.5(17)
Z	18	2	1
D_{calcd} (g·cm^{-3})	1.488	1.741	1.722
Absorption coefficient (mm^{-1})	1.448	2.172	0.954
F(000)	3528	388	333
Crystal size/mm^3	0.34 x 0.14 x 0.11	0.25 x 0.21 x 0.11	0.36 x 0.25 x 0.18
θ range for data collection/ °	1.592–24.994	6.352–73.454	2.618–25.004
Limiting indices	-27 < =h < =27, −27 < =k < =26, −19 < =l < =19	-9 < =h < =8, −12 < =k < =8, −6 < =l < =11	−8 < =h < =8, −9 < =k < =9, −13 < =l < =13
Reflections collected/unique	17216/3040 [R (int) = 0.0964]	4127/1403 [R (int) = 0.0427]	13127/2221 [R (int) = 0.0319]
Data/restraints/parameters	3040/0/226	1403/0/115	2221/8/200
Goodness-of-fit on F^2	1.047	1.040	1.027
Final R indices [*I* > 2sigma(I)]	R1 = 0.0516, wR2 = 0.1799	R1 = 0.0447, wR2 = 0.1236	R1 = 0.0466, wR2 = 0.1674
R indices (all data)	R1 = 0.0812, wR2 = 0.2019	R1 = 0.0459, wR2 = 0.1249	R1 = 0.0506, wR2 = 0.1702
Largest diff. Peak and hole(e. Å^{-3})	1.834and −0.368	0.576and −0.842	0.338 and − 0.525
CCDCNO.	1832414	1958466	1958467

hybrid orbitals. In the [NiO_2N_4], four N atoms (N1, N3, N1A, N3B) from four different 2,6-bip ligands and two O atoms (O1, O1A) from two 2,6-bip ligands are attached to Ni (II) ion. The Ni-N bond distances range from 2.0908(15) to 2.1410(16) Å, and the Ni-O bond distance is 2.1025(13) Å. The distances of Ni-O1A/N1A are 2.1025(13)/2.1410(16) Å, slightly larger, which can be ascribed to the tension of the quaternion chelating ring. The N1, N1A, O1 and O1A are located in the equatorial plane, while N3 and N3B occupy the axial positions. The O-Ni1-O bond angle is 180.0°, the O-Ni1-N bond angle range is 63.50(5) ° to 116.50(5) °, and the N-Ni1-N bond angle range is 89.99(6) ° to 180.00(3) °. The 2,6-bip ligand adopts the $\mu_2:\eta^1\eta^1\eta^1$ coordination mode, which is different from that in **1**. One N atom on the imidazole ring coordinates with the Ni (II) ion, while one N atom and one O atom on the pyridone ring chelate the Ni (II) ion. The dihedral angle of the imidazole ring and the pyridone ring in 2,6-bip ligand is 29.46 °. The two adjacent Ni (II) ions are bridged by 2,6-bip ligand to form a 1D chain with the Ni ... Ni distance of 7.696 Å. The 1D chains are connected by 2,6-bip ligands to form a 2D network

TABLE 2 Selected bond lengths [Å] and angles [°] for coordination polymers **1–3**

1			
Zn(1)-O(2)	1.981(4)	Zn(1)-N(3)A	2.029(5)
Zn(1)-O(1)	1.957(4)	Zn(1)-N(6)B	2.035(5)
O(2)-Zn(1)-N(3)A	95.42(18)	O(1)-Zn(1)-N(3)A	109.87(18)
O(2)-Zn(1)-N(6)B	112.12(19)	O(1)-Zn(1)-N(6)B	97.25(18)
O(1)-Zn(1)-O(2)	133.39(17)	N(3)A-Zn(1)-N(6)B	107.3(2)
2			
Ni(1)-O(1)A	2.1025(13)	Ni(1)-N(1)A	2.1410(16)
Ni(1)-O(1)	2.1025(13)	Ni(1)-N(3)B	2.0909(15)
Ni(1)-N(1)A	2.1410(16)	Ni(1)-N(3)	2.0908(15)
O(1)-Ni(1)-O(1)A	180.0	N(3)B-Ni(1)-O(1)	89.62(6)
O(1)-Ni(1)-N(1)	63.50(5)	N(3)-Ni(1)-O(1)	90.38(6)
O(1)A-Ni(1)-N(1)	116.50(5)	N(3)-Ni(1)-N(1)	90.01(6)
O(1)-Ni(1)-N(1)A	116.50(5)	N(3)B-Ni(1)-N(1)A	90.01(6)
O(1)A-Ni(1)-N(1)A	63.50(5)	N(3)B-Ni(1)-N(1)	89.99(6)
N(1)-Ni(1)-N(1)A	180.00(3)	N(3)-Ni(1)-N(1)A	89.99(6)
N(3)B-Ni(1)-O(1)A	90.38(6)	N(3)-Ni(1)-N(3)B	180.0
N(3)-Ni(1)-O(1)A	89.62(6)		
3			
Cu(1)-O(3)	1.944(4)	Cu(1)-N(3)	1.976(4)
Cu(1)-O(3)A	1.944(4)	Cu(1)-N(3)A	1.976(4)
O(3)-Cu(1)-O(3)A	180.0	O(3)-Cu(1)-N(3)	89.11(15)
O(3)A-Cu(1)-N(3)	90.89(15)	O(3)A-Cu(1)-N(3)A	89.11(15)
O(3)-Cu(1)-N(3)A	90.89(15)	N(3)-Cu(1)-N(3)A	180.0

Symmetry transformations used to generate equivalent atoms:
For **1**: A: -x + y + 2/3, −x + 4/3, z + 1/3; B: y-1/3, −x + y + 1/3, −z + 4/3
For **2**: A: x + 1/2, −y + 1/2, z + 1/2; B: -x + 2, −y, −z + 1
For **3**: A: -x, −y, −z + 1

structure, in which the [NiO_2N_4] acts as a node, and the 2,6-bip ligand acts as a linker (Figure 2b).

Structure of 3. Coordination polymer **3** is a 1D chain structure, belonging to the triclinic system, and the space group $P\bar{1}$. The asymmetric unit of **3** contains one Cu (II) ion, one tfbdc ligand, two 2,6-bipH ligands, and two free H_2O molecules. As shown in Figure 3a, Cu (II) ion adopts a [CuO_2N_2] parallelogram coordination geometry by Cu dsp^3 hybrid orbitals. The Cu (II) ion is surrounded by two O atoms (O3, O3A) from two tfbdc ligands and two N atoms (N3, N3A) from two 2,6-bipH ligands. The Cu-O and Cu-N bond lengths are 1.944(4) and 1.976(4) Å, respectively. The O-Cu1-O/N-Cu1-N bond angle is 180.0 °, and the O-Cu1-N bond angle range is 89.11(15) °~90.89(15) °. Unlike complexes **1** and **2,** [CuO_2N_2] acts as a node while the tfbdc ligand acts as linker in **3**. The tfbdc ligand bridges Cu (II) ions by a $\mu_1{:}\eta^1\eta^0/\mu_1{:}\eta^1\eta^0$ coordination mode to form a 1D chain along the c-axis with the Cu … Cu distance of 11.002 Å and the Cu … Cu … Cu bond angle of 180 ° (Figure 3b). In tfbdc, the carboxyl group on the benzene ring is twisted, with a dihedral angle of 54.12° between the carboxyl plane and the benzene ring. The 2,6-bipH as a monodentate ligand adopts the $\mu_1{:}\eta^1\eta^0\eta^0$ coordination mode, and only one N atom on the imidazole ring coordinate with Cu (II) ion. The hydroxyl group of the 2,6-bipH ligand is not deprotonated. The dihedral angle of the imidazole ring and the pyridone ring is 6.49 °. The H atom on the imidazole ring of the 2,6-bipH ligand forms a hydrogen bond with the F atom of tfbdc. The C8-H8 … F2 hydrogen bond distance is 3.1998(7) Å, and the bond angle is 121.417(2) °. A hydrogen bond O1-H1 … O1A is also formed between the hydroxyl groups of the 2,6-bipH ligands with the hydrogen bond distance of 2.6623(6) Å and the bond angle of 85.58 (2) °.

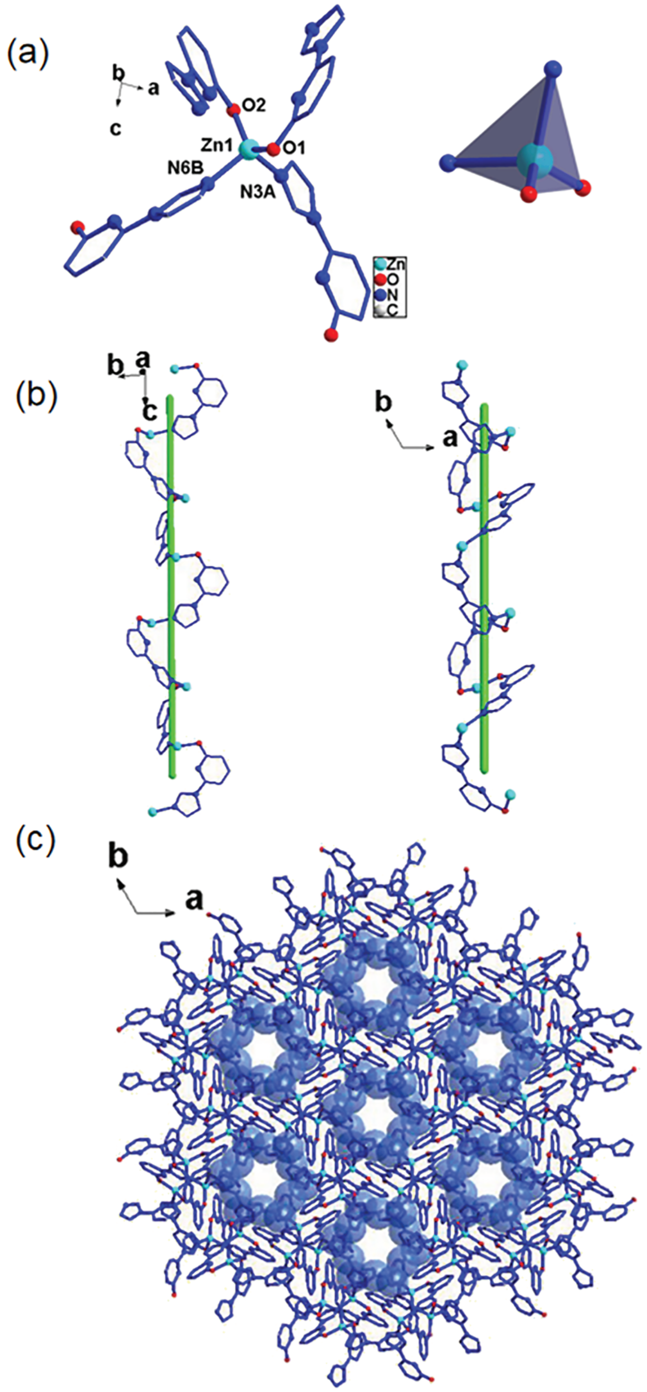

FIGURE 1 The structure of **1**: (a) the coordination environment of the Zn (II) ion; (b) Left-type Zn-(2,6-bip) helical chain (left) and Right-type Zn-(2,6-bip) helical chain (right), (c) 3D framework

The hydrogen bonds connect the 1D chains to construct a 3D supramolecular structure (Figure 3c).

Discussions. The three synthesized coordination polymers show different structures from 3D to 1D, which are resulted from the different single-metal ion "node" and "linker" coordination modes. Zn/Ni/Cu adopt different constructions, tetra-coordinated Zn, hexa-coordinated Ni, and tetra-coordinated Cu. The coordination number of Ni is greater than that of Zn and Cu, which can be ascribed to the larger radius of Ni than those of Zn and Cu. Zn/Ni/Cu use different hybrid orbitals, sp^3 for Zn, d^2sp^3 for Ni, and dsp^2 for Cu to form $[ZnO_2N_2]$ tetrahedron, $[NiO_2N_4]$ octahedron, and $[CuO_2N_2]$ parallelogram, which acts as the single-metal ion "node" in structure. The linker 2,6-bipH has three coordination atoms, which can adopt different coordination modes, namely μ_2:$\eta^1\eta^1\eta^0$ in **1**, μ_2:$\eta^1\eta^1\eta^1$ in **2**, and μ_1:$\eta^1\eta^0\eta^0$ in **3**. However, the H_2tfbdc ligand only coordinates with Cu (**II**) ion in **3**, H_2tfbdc ligand may play the role of template in the synthesis of **1** and **2**. We can conclude that differences in the constructions of center metal and ligand coordination modes result in the formation of different dimensional structures, e.g. 3D framework (**1**), 2D network (**2**), and 1D chain (**3**) structures. The presence of hydrogen bonds in **3** leads the formation of high-dimensional supermolecular structure. It is interesting to note that the high-dimensional coordination polymer **1** features a micropore with the pore volume of 14.2% (based on PLATON calculation).

3.2 | Thermal stability of coordination polymers 1–3

The phase purity of **1**, **2** and **3** were confirmed by powder X-ray diffraction (PXRD) analysis. The powder X-ray diffraction (PXRD) patterns of synthesized samples **1–3** fit well with the simulation plots, indicating that all coordination polymers are in pure phase (Figure 4 and Figure S1). In order to measuring their thermal stability, samples **1–3** were subjected to thermogravimetric analysis (TGA) at a heating rate of 10 °C•min^{-1}. As shown in Figure S2, the TGA curves of coordination polymers **1** and **2** below 275 °C and 300 °C, respectively, are substantially stable, indicating that **1** and **2** are stable under 275 °C for **1** and 300 °C for **2**. When the temperatures further rise form 275 °C for **1** and 300 °C for **2**, the frameworks of **1** and **2** begin to decompose. The TGA curves show that the total loss is 72.32% for **1** and 79.84% for **2**. The final residuals of **1** and **2** after thermal decomposition are ZnO (calculated value: 79.00%) for **1** and NiO (calculated value: 80.30%) for **2**. For **3**, the first loss is observed on the TGA curve between the temperature of 100 and 150 °C, and the weight loss is about 5.81%, corresponding to the loss of water molecules (calculated value: 5.47%). The TGA curve starts a second drop at 190 °C with the total loss of 87.74%, indicating that the final residual is CuO (calculated value: 87.84%).

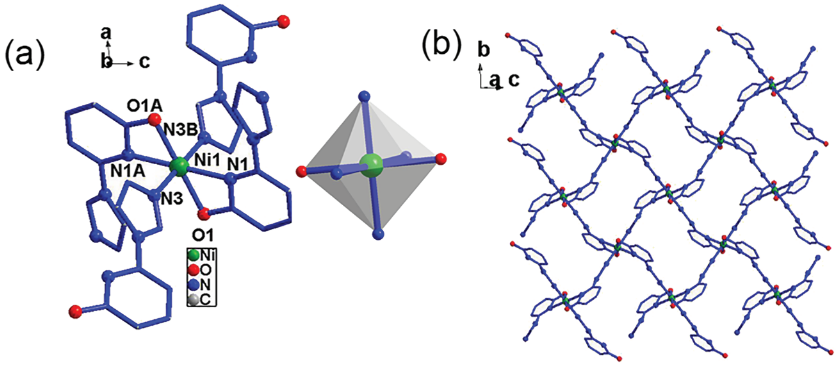

FIGURE 2 The structure of **2**: (a) the coordination environment of the Ni (II) ion; (b) 2D network

3.3 | Luminescence properties

As Zn-CP with d^{10} electronic construction often shows interesting luminescence properties, while Cu (II) and Ni (II)-CPs with open shells often show quenching luminescence.[3] So, the luminescence properties of **1** and free 2,6-bipH ligand were studied (Figure 5). The spectrum shows that 2,6-bipH ligand exhibits a broad emission band with the maximum emission intensity at 428 nm upon the excitation at 352 nm. The spectrum of **1** displays strong blue emission band from 375 to 500 nm upon the excitation at 340 nm. The maximum emission is at 412 nm, which is close to that of the free 2,6-bipH ligand. The center Zn (II) with d^{10} electronic configuration couldn't accept π electron easily.[48] Therefore, the blue emission of **1** can be attributed to the $\pi^* \rightarrow \pi$ transition of the 2,6-bipH ligand. Compared with 2,6-bipH ligand, **1** shows much stronger emission and a significant blue shift of 16 nm for maximum emission. Emission intensities of the free ligand and ligand within the coordination polymer are different significantly. Additionally, the ligand within the coordination polymer may enforce a molecular conformation of the ligand, resulting in an

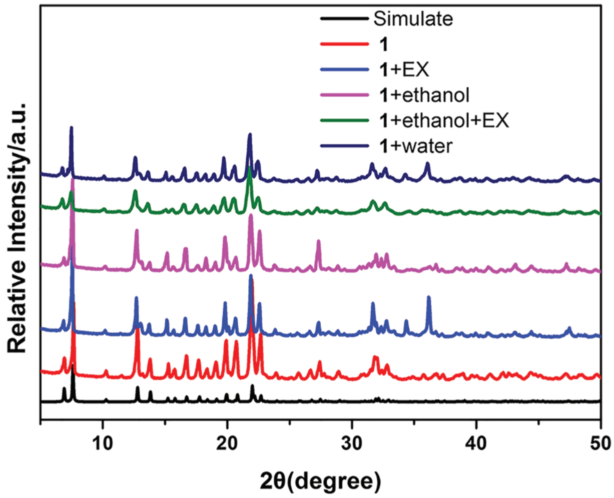

FIGURE 4 The PXRD patterns of coordination polymer **1**

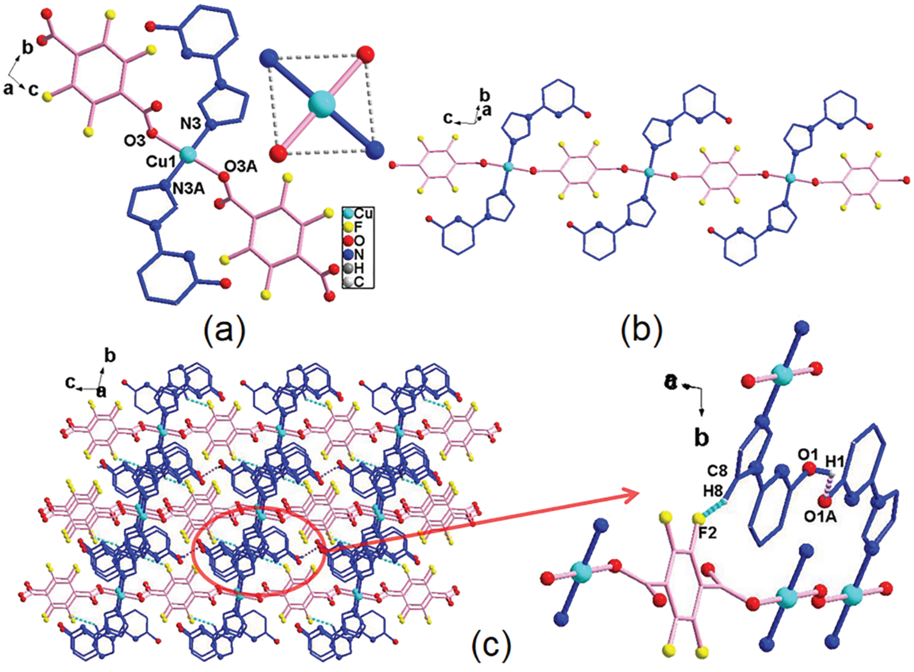

FIGURE 3 The structure of **3**: (a) the coordination environment of the Cu (II) ion; (b) 1D chain structure; (c) 2D supramolecular structure and the hydrogen bonds

increase in the non-radiation deactivating effect, and further contribute to stronger emission.[3,48–50] The good luminescence properties of **1** makes it possible in the field of luminescence detection.

3.4 | Luminescence properties of 1 in solvents

When coordination polymer **1** is immersed in water or ethanol, the powder X-ray diffraction (PXRD) patterns still fit well with the simulation plot, which indicates **1** has good chemical stability in solvents (Figure 4). The luminescence properties of **1** in common solvents are further discussed. Coordination polymer **1** powder sample (3 mg) was dispersed in solvents (3 ml) to make suspensions by ultrasonication, where the used solvents include ethanol, acetonitrile, water, dimethyl sulfoxide (DMSO), acetone, N,N-dimethylformamide (DMF), trichloromethane and methanol. The luminescence spectra of these suspensions are obtained at the maximum excitation wavelength of 340 nm. As shown in Figure 6, an emission band of **1** is observed in all suspensions, and the maximum value is at 412 nm with relatively high intensity, indicating that **1** maintains good luminescence properties in these solvents. When coordination polymer **1** is dispersed in ethanol, the strongest luminescence can be obtained, compared with all other suspensions. This means that **1** has potential luminescence detection application in solvent systems.

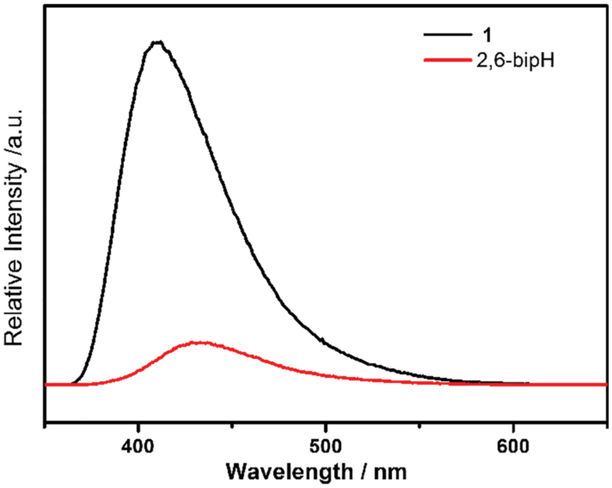

FIGURE 5 The solid state emission spectra of **1** and the free ligand

3.5 | Luminescent sensing

Considering the good luminescence properties and stability of **1**, it can be used as a luminescent sensor. To test the capability of **1** in sensing different antibiotics, its luminescence properties were tested in ethanol solution with the different antibiotics, including ciprofloxacin (CX), pefloxacin (PX), levofloxacin (LX), falofloxacin (FX), and enoxacin (EX) (Figure S3). The emission spectra of suspensions (3 mg **1** in 3 ml 0.01 M ethanol solution of the different antibiotics) were measured at the excitation wavelength of 340 nm. As shown in Figure 7, different antibiotics have different degrees of influence on the luminescence intensity of **1**, compared with the blank ethanol suspension. The emission of all suspensions is reduced. The luminescence quenching efficiency of **1** by FX, LX, PX and CX is 34.05%, 61.74%, 76.02%, and 82.47%, respectively. And the position of maximum emission shows a red shift with different degree. It is worth noting that the luminescence quenching efficiency of **1** by EX is 88.20%. Therefore, the detection result of EX is better than those of other antibiotics. Thus, coordination polymer **1** can be used as the luminescence sensor to detect EX. To further explore the quenching effect of luminescence of **1** with EX, luminescence titration experiment was carried out by adding EX step-by-step to the coordination polymer **1** ethanol suspension, and the emission intensity at 412 nm was monitored. When the

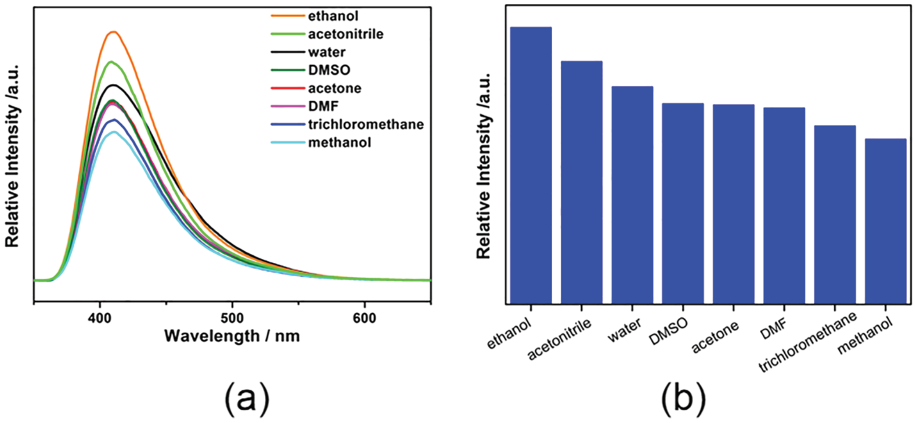

FIGURE 6 Emission spectra (a) and the transition intensity (b) of **1** dispersed in different solvents (λex =340 nm)

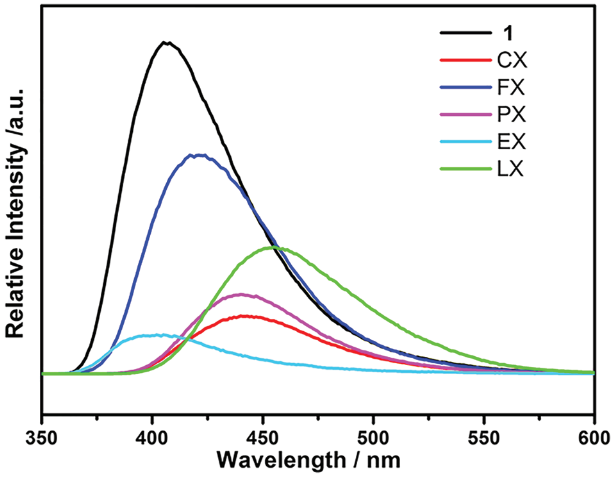

FIGURE 7 Luminescent spectra of **1** upon the addition of different antibiotics (CXEXFXLXPX, 10^{-2} M) ethanol solutions

TABLE 3 Comparison of other methods for detection EX

Method	LOD	Ref
HPLC	1.09 μg•L^{-1}	[32]
UHPLC	40 μg•L^{-1}	[34]
RLS-HPLC	5.1 ng•mL	[33]
ECL	0.02 μg•mL^{-1}	[31]
ECL	3.2×10^{-7} mol•L^{-1}	[30]

volume of EX ethanol solution(10^{-3} mol·L^{-1}) increases from 0 to 270 μL, it can be observed that the emission intensity of **1** is gradually reduced (Figure 8a). The luminescence quenching efficiency can be analyzed by the Stern–Volmer (SV) equation $I_0/I\text{-}1 = K_{SV}[A]$[51] ($K_{SV}$, the quenching constant; [A], the molar concentration of EX; I_0 and I, the luminescence intensities before and after the addition of EX, respectively). As depicted in Figure 8b, the SV plot is almost linear, and the calculated K_{SV} is 4.2259×10^4 M^{-1} with a linear fit coefficient value of 0.9903. Moreover, the detection limit ($3\sigma/K_{SV}$) of **1** toward EX is calculated (σ: standard error for three repeated luminescence measurements of blank solution, $\sigma = 0.509$) to be 3.61×10^{-5} M.

The sensing performances of other method toward EX are listed in Table 3. These methods, including HPLC (high performance liquid chromatography)/ECL (Electrochemiluminescence)/RLS-HPLC (high performance liquid chromatography technique incorporating resonance light scattering)/FL-CPs, can be used to detect EX. Remarkably, **1** is represented to be the first CPs-based luminescence sensor for EX detection. The detection limit is 3.61×10^{-5} M. The results show that **1** can be used as a luminescent sensor to detect EX.

3.6 | Luminescence quenching mechanism

In order to clearly understand the effect of EX on the luminescence of **1**, the possible quenching mechanisms were explored. Firstly, the simulated PXRD patterns and the one after being immersed in EX fit well (Figure 4). The result indicates that the 3D structure of **1** remains intact when adding EX. Therefore, the luminescence quenching of **1** shows no obvious connections to the collapse of the framework.[52] In order to further explore the quenching mechanism of **1** in the presence of EX, the UV–vis absorption spectrum of the EX solution was measured. The absorption spectrum of EX solution and the emission spectrum of the **1** are compared. It could be seen that they have no overlaps (Figure 9). Therefore, the energy transfer **1** to EX is excluded. It is observed by the UV–vis absorption spectrum of EX that there is strong absorption at 262 nm and 336 nm. It is worth noting that the absorption of EX at 336 nm coincides with the excitation spectrum of **1** partially. The reason for luminescence quenching may be that the absorption of EX at 336 nm inhibits the absorption of excitation energy of **1**. To verify this mechanism, the effect of EX on the luminescence of **1** was examined at an excitation wavelength of 380 nm (which is out of the range of EX absorption). The results show that the luminescence quenching also occurred

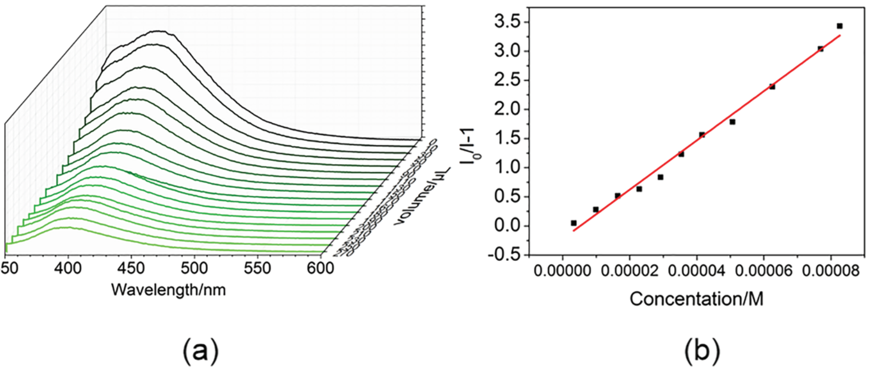

FIGURE 8 (a) Luminescent spectra of **1** ethanol solutions with different concentrations of EX (λex = 340 nm); (b) The sterm-volmer plot of **1** for EX (λex = 340 nm)

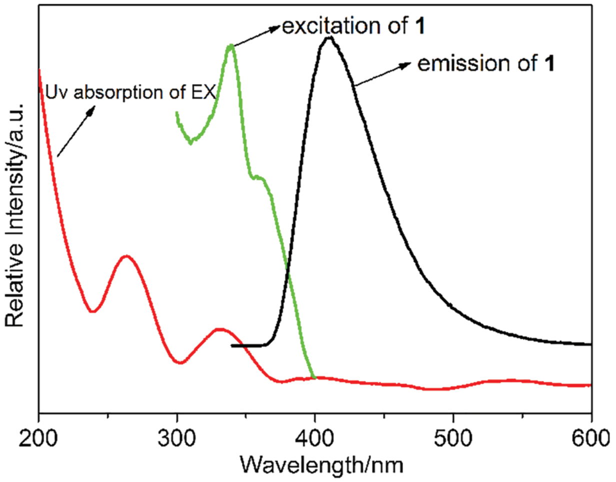

FIGURE 9 Excitation and emission spectra of EX and UV–vis absorption spectrum of EX

(Figure 10). The K_{SV} of $1.4759 \times 10^3\ M^{-1}$ is calculated, which is less significant than upon 340 nm excitation ($K_{SV} = 4.2259 \times 10^4\ M^{-1}$). The difference in quenching constant indicates that the absorption of EX at the excitation wavelength partially affects the luminescence quenching of **1**.[53]

TABLE 4 The LUMO and HUMO energies of the fluoroquinolones

	CX	EX	PX	FX	LX
HOMO/ev	−3.399	−5.77	−5.780	−5.631	−5.398
LUMO/ev	−2.305	−1.438	−1.399	−1.421	−1.278

Another possible mechanism for the luminescence quenching is photoinduced electron transfer (PET).[54–56] Since the luminescence of **1** can be attributed to the $\pi^* \rightarrow \pi$ transition of the 2,6-bipH ligand, the luminescence quenching may be due to the PET between 2,6-bipH ligand and EX. When the lowest-unoccupied-molecular-orbital (LUMO) energy level of the fluoroquinolones is lower than that of 2,6-bipH ligand, electrons can be transferred from the LUMO of the 2,6-bipH ligand to the LUMO of fluoroquinolone antibiotics upon excitation to cause luminescence quenching. To explore the conjecture, the highest-occupied-molecular-orbital (HOMO) and LUMO of the fluoroquinolones was calculated (Table 4). The calculated LUMO energy of 2,6-bipH ligand (−1.1 eV) is higher than that of EX (−1.437 eV) (Figure 11), which makes the electron transfer from LUMO orbit of 2,6-bipH ligand to the LUMO orbit of EX much easier. Therefore, the luminescence quenching occurs. Therefore, both the PET process and the absorption of EX at excitation wavelength (336 nm) contribute to the luminescence quenching of **1**.

Discussion. Coordination polymers **1–3** are the first synthesized complexes containing the 2,6-bipH ligand, and such complexes are not reported in the literatures. Several Zn/Ni/Cu-complexes with polycarboxylic acid and/or N-donor ligands have been synthesized by our laboratory, such as 3D $[Zn\ (dpdc)(btb)_{0.5}]_n$ and $[Cu_3(dpdc)_3(btb)_2]_n$ with $[ZnO_4N]$ and $[Cu1O_5]/[Cu2O_4N_2]$ polyhedra, respectively[57]; 3D $[Cu_2(O\text{-}cpia)(btb)_{0.5}{\bullet}(OH)]$, 3D $[Cu_3(O\text{-}cpia)_2(bpy)_2]$, 2D $[Ni_2(O\text{-}cpia)(phen){\bullet}(OH){\bullet}H_2O]{\bullet}2H_2O$ and 3D $[Ni_3(O\text{-}cpia)_2(bpy)_3{\bullet}2H_2O]{\bullet}2H_2O$ with $[Cu1O_4N]/[Cu2O_5]$,

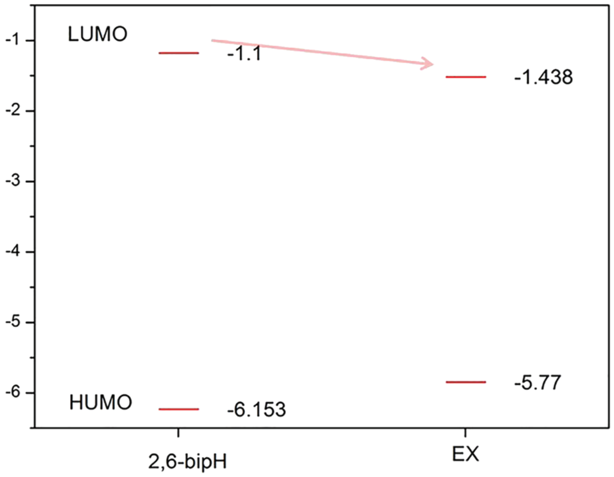

FIGURE 11 The calculated LUMO and HUMO energy of 2,6-bipH ligand and EX

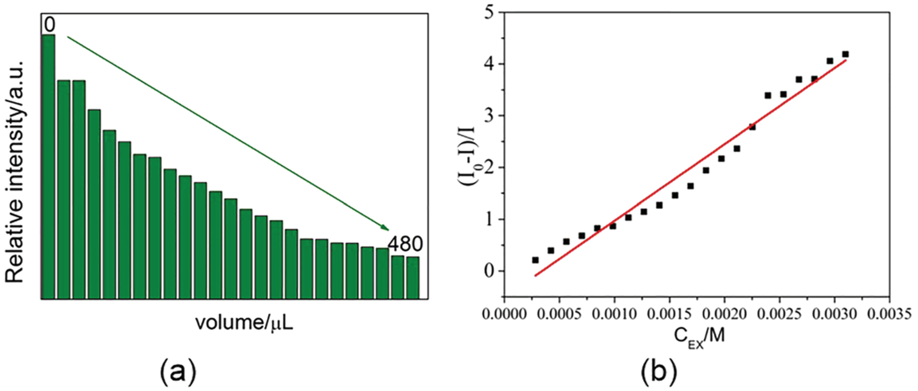

FIGURE 10 (a) Luminescent spectra of **1** in ethanol solution with different concentrations of EX (λex = 380 nm); (b) The sterm-volmer plot of **1** for EX (λex = 380 nm)

$[Cu1O_3N_2]/[Cu2O_4]$, $[Ni1O_4N_2]/[Ni2O_6]$, and $[Ni1O_4N]/[Ni2O_4N_2]$ polyhedra, respectively[58]; 3D [Zn(3,3′-dpdc) bpp] and $[Cu_2(3,3'\text{-dpdc})_2(bpp)]$ with $[ZnO_4N]$ and $[CuO_4N]$ polyhedra, respectively.[59] These complexes show different interesting structural features consisting of different metal ion (Zn (II), Cu (II) and Ni (II)) configurations, which show catalysis or luminescence property. Zn-complexes exhibit ligand-based blue luminescence and can be used as luminescent sensors, reflecting the luminescent sensing ability for different analytes, such as for Fe^{3+} and Tb^{3+} ion. Coordination polymers **1–3** have different structures from these complexes. Especially, coordination polymer **1** can detect enoxacin in ethanol solution with a low detection limit.

4 | CONCLUSIONS

In summary, three coordination polymers, $[M(2,6\text{-bip})_2]$ (M = Zn (**1**), Ni (**2**)) and $[Cu\ (tfbdc)(2,6\text{-bipH})_2]\bullet 2H_2O$ (**3**), have been synthesized and characterized. The tfbdc ligand is bound to Cu ions in **3**, whereas it is uncoordinated to Zn in **1** and Ni in **2**, tfbdc ligand may play the template role in the synthesis of **1** and **2**. The 2,6-bip or 2,6-bipH ligand adopts different coordination modes in the three coordination polymers. The different polyhedral units of metal ions (tetrahedron for Zn, octahedron for Ni, and parallelogram for Cu) are linked by ligands to form the diverse structures of the coordination polymers, 3D architecture (**1**), 2D network (**2**), and 1D chain (**3**). Interestingly, **1** exhibits high emission in ethanol and can be used as a luminescent sensor for the detection of EX in ethanol solution. The detection limit is 3.61×10^{-5} M. The sensing mechanisms may be attributed to the PET process and the absorption of EX at excitation.

ACKNOWLEDGMENTS

The authors are grateful to the Key project of science and technology plan of Beijing Education Commission (KZ201910028038), the National Natural Science Foundation of China (21471104), and Laboratory Open Project Fund of Capital Normal University (LIP18009S047).

CONFLICT OF INTEREST

There are no conflicts to declare.

ORCID

Xia Li https://orcid.org/0000-0002-1110-0117

REFERENCES

[1] J. R. Li, J. Sculley, H. C. Zhou, *Chem. Rev.* **2012**, *112*, 869.
[2] J. R. Li, R. J. Kuppler, H. C. Zhou, *Chem. Soc. Rev.* **2009**, *38*, 1477.
[3] J. Heine, K. Muller-Buschbaum, *Chem. Soc. Rev.* **2013**, *42*, 9232.
[4] X. L. Qu, B. Yan, *Inorg. Chem.* **2019**, *58*, 524.
[5] J. M. Li, R. Huo, X. Li, H. L. Sun, *Inorg. Chem.* **2019**, *58*, 9855.
[6] Z. Li, S. Zhang, R. Xu, Q. Zhang, Z. Wang, C. Fu, *Appl. Organomet. Chem.* **2019**, 33.
[7] G. Sargazi, D. Afzali, A. Mostafavi, *Appl. Organomet. Chem.* **2019**, *33*, e4816.
[8] S. Yuan, L. Zou, J. S. Qin, J. Li, L. Huang, L. Feng, X. Wang, M. Bosch, A. Alsalme, T. Cagin, H. C. Zhou, *Nat. Commun.* **2017**, *8*, 15356.
[9] S. Millan, B. Gil-Hernandez, E. Milles, S. Gokpinar, G. Makhloufi, A. Schmitz, C. Schlusener, C. Janiak, *Dalton Trans.* **2019**, *48*, 8057.
[10] D. J. Tranchemontagne, J. L. Mendoza-Cortes, M. O'Keeffe, O. M. Yaghi, *Chem. Soc. Rev.* **2009**, *38*, 1257.
[11] Q. Ding, Y. Pan, Y. Luo, M. Zhou, Y. Guan, B. Li, M. Trivedi, A. Kumar, J. Liu, *ACS Omega.* **2019**, *4*, 10775.
[12] W. Lu, Z. Wei, Z. Y. Gu, T. F. Liu, J. Park, J. Park, J. Tian, M. Zhang, Q. Zhang, T. Gentle III, *Chem. Soc. Rev.* **2014**, *43*, 5561.
[13] Z. J. Lin, J. Lu, M. Hong, R. Cao, *Chem. Soc. Rev.* **2014**, *43*, 5867.
[14] C. Y. Sun, S. X. Liu, D. D. Liang, K. Z. Shao, Y. H. Ren, Z. M. Su, *J. Am. Chem. Soc.* **2009**, *131*, 1883.
[15] M. Eddaoudi, D. F. Sava, J. F. Eubank, K. Adil, V. Guillerm, *Chem. Soc. Rev.* **2015**, *44*, 228.
[16] B. Li, H. M. Wen, Y. Cui, G. Qian, B. Chen, *Prog. Polym. Sci.* **2015**, *48*, 40.
[17] X. Zhao, S. Wang, L. Zhang, S. Liu, G. Yuan, *Inorg. Chem.* **2019**, *58*, 2444.
[18] H. Furukawa, J. Kim, N. W. Ockwig, M. O'Keeffe, O. M. Yaghi, *J. Am. Chem. Soc.* **2008**, *130*, 11650.
[19] D. Niu, J. Yang, J. Guo, W. Q. Kan, S. Y. Song, P. Du, J. F. Ma, *Cryst. Growth des.* **2012**, *12*, 2397.
[20] J. Guo, J. Yang, Y. Y. Liu, J. F. Ma, *CrystEngComm* **2012**, *14*, 6609.
[21] Z. W. Zhai, S. H. Yang, M. Cao, L. K. Li, C. X. Du, S. Q. Zang, *Cryst. Growth des.* **2018**, *18*, 7173.
[22] G. C. Liu, Y. Li, J. Chi, N. Xu, X. L. Wang, H. Y. Lin, Y. Q. Chen, *Dyes Pigm.* **2020**, *174*, 108064.
[23] Y. D. Farahani, V. Safarifard, *J. Solid State Chem.* **2019**, *275*, 131.
[24] F. Cheng, R. Fu, Y. Wen, Y. Y. Yang, C. Zeng, Y. Zhang, S. Hu, X. Wu, *J. Mater. Chem. C* **2018**, *6*, 12341.
[25] P. Das, S. K. Mandal, *J. Mater. Chem. A* **2018**, *6*, 21274.
[26] P. Rocio-Bautista, V. Pino, J. Pasan, I. Lopez-Hernandez, J. H. Ayala, C. Ruiz-Perez, A. M. Afonso, *Talanta* **2018**, *179*, 775.
[27] J. Lu, X. H. Xin, Y. J. Lin, S. H. Wang, J. G. Xu, F. K. Zheng, G. C. Guo, *Dalton Trans.* **2019**, *48*, 1722.
[28] F. Y. Yi, S. C. Wang, M. Gu, J. Q. Zheng, L. Han, *J. Mater. Chem. C* **2018**, *6*, 2010.
[29] S. S. Zhao, J. Yang, Y. Y. Liu, J. F. Ma, *Inorg. Chem.* **2016**, *55*, 2261.
[30] Y. M. Liu, Y. M. Shi, Z. L. Liu, *Biomed. Chromatogr.* **2010**, *24*, 941.

[31] M. Su, *J. Pharm. Pharm. Sci.* **2017**, *6*, 1274.

[32] S. Seyhan Bozkurt, D. Erdogan, M. Antep, N. Tuzmen, M. Merdivan, *J. Liq. Chromatogr. R. T.* **2016**, *39*, 21.

[33] Z. Pan, J. Peng, Y. Chen, X. Zang, H. Peng, L. Bu, H. Xiao, Y. He, F. Chen, Y. Chen, *Microchem. J.* **2018**, *136*, 71.

[34] N. Arroyo-Manzanares, J. F. Huertas-Pérez, M. Lombardo-Agüí, L. Gámiz-Gracia, A. M. García-Campaña, *Anal. Methods-UK.* **2015**, *7*, 253.

[35] A. Ma, J. Wu, Y. Han, F. Chen, B. Li, S. Cai, H. Huang, A. Singh, A. Kumar, J. Liu, *Dalton Trans.* **2018**, *47*, 9627.

[36] R. X. Yao, X. Cui, X. X. Jia, F. Q. Zhang, X. M. Zhang, *Inorg. Chem.* **2016**, *55*, 9270.

[37] L. Li, X. Cao, R. Huang, *Chin. J. Chem.* **2016**, *34*, 143.

[38] X. Gao, M. Zheng, L. Qin, K. Shen, H. Zheng, *Cryst. Growth des.* **2016**, *16*, 4711.

[39] G. C. Liu, Y. Li, Z. J. Lu, X. W. Li, X. Wang, X. Wang, X. X. Chen, *CrystEngComm* **2019**, *21*, 5344.

[40] R. P. Ye, X. Zhang, J. Q. Zhai, Y. Y. Qin, L. Zhang, Y. G. Yao, J. Zhang, *CrystEngComm* **2015**, *17*, 9155.

[41] J. X. Ma, Z. Yang, T. Zhou, Q. Guo, J. Yang, T. Yang, Q. Yang, *New J. Chem.* **2018**, *42*, 15413.

[42] C. C. Chiu, F. K. Shieh, H. G. Tsai, *Inorg. Chem.* **2019**, *58*, 14457.

[43] X. Wang, X. Liu, H. Rong, Y. Song, H. Wen, Q. Liu, *RSC Adv.* **2017**, *7*, 29611.

[44] Z. J. Wang, L. Qin, X. Zhang, J. X. Chen, H. G. Zheng, *Cryst. Growth des.* **2015**, *15*, 1303.

[45] G. M. Sheldrick, SHELXS–97, Program for Crystal Structure Refinement, University of Göttingen, **1997**.

[46] G. M. Sheldrick, SHELXL-97, Program for Crystal Structure Solution, University of Göttingen, **1997**.

[47] L. Spek, *J. Appl. Crystallogr.* **2003**, *36*, 7.

[48] Z. Zhou, M. L. Han, H. R. Fu, L. F. Ma, F. Luo, D. S. Li, *Dalton Trans.* **2018**, *47*, 5359.

[49] Y. Bing, M. Yu, M. Hu, *RSC Adv.* **2015**, *5*, 47216.

[50] Y. Pan, J. Wang, X. Guo, X. Liu, X. Tang, H. Zhang, *J. Colloid Interface Sci.* **2018**, *513*, 418.

[51] J. M. Li, R. Li, X. Li, *CrystEngComm* **2018**, *20*, 4962.

[52] X. M. Kang, R. R. Cheng, H. Xu, W. M. Wang, B. Zhao, *Chem. – Eur. J.* **2017**, *23*, 13289.

[53] X. D. Zhu, K. Zhang, Y. Wang, W. W. Long, R. J. Sa, T. F. Liu, J. Lu, *Inorg. Chem.* **2018**, *57*, 1060.

[54] J. Xiao, J. Liu, X. Gao, G. Ji, D. Wang, Z. Liu, *Sens. Actuators B Chem.* **2018**, *269*, 164.

[55] H. Malik, P. K. Iyer, *ACS Appl. Mater. Interfaces* **2017**, *9*, 4433.

[56] X. Zhang, Z. Zhan, X. Liang, C. Chen, X. Liu, Y. Jia, M. Hu, *Dalton Trans.* **2018**, *47*, 3272.

[57] M. N. Zhang, T. T. Fan, Q. S. Wang, H. L. Han, X. Li, *J. Solid State Chem.* **2018**, *258*, 744.

[58] Q. W. Xu, Q. S. Wang, S. S. Li, X. Li, *RSC Adv.* **2019**, *9*, 16305.

[59] T. T. Fan, J. J. Li, X. L. Qu, H. L. Han, X. Li, *CrystEngComm* **2015**, *17*, 9443.

SUPPORTING INFORMATION

Additional supporting information may be found online in the Supporting Information section at the end of this article.

How to cite this article: Li S, Zhou X, Xu Q, Liu D, Cui R, Li X. Transition Metal–organic Coordination Polymers Containing 6-(1H-imidazol-1-yl)-2(1H)-Pyridinone: Synthesis, Structure and Fluorescent Sensing for Enoxacin. *Appl Organometal Chem*. 2020;e5566. https://doi.org/10.1002/aoc.5566